IN-71
1708
817

NASA Technical Memorandum 103606
AIAA-90-4022

Unsteady Blade Pressure Measurements for the SR-7A Propeller at Cruise Conditions

L.J. Heidelberg
Lewis Research Center
Cleveland, Ohio

and

M. Nallasamy
Sverdrup Technology, Inc.
Lewis Research Center Group
Brook Park, Ohio

Prepared for the
13th Aeroacoustics Conference
sponsored by the American Institute of Aeronautics and Astronautics
Tallahassee, Florida, October 22-24, 1990

NASA

UNSTEADY BLADE PRESSURE MEASUREMENTS FOR THE SR-7A PROPELLER AT CRUISE CONDITIONS

L.J. Heidelberg
National Administration and Space Administration
Lewis Research Center
Cleveland, Ohio 44135-3191

and

M. Nallasamy
Sverdrup Technology, Inc.
Lewis Research Center Group
Brook Park, Ohio 44142

SUMMARY

The unsteady blade surface pressures were measured on the SR-7A propeller. The freestream Mach number, inflow angle, and advance ratio were varied while measurements were made at nine blade stations. At a freestream Mach number of 0.8, the data in terms of unsteady pressure coefficient versus azimuth angle is compared to an unsteady three-dimensional Euler solution. This comparison of waveforms with the code yielded very encouraging results. The code predicts the shape (phase) of the waveform very well while the magnitude is over-predicted in many cases. At tunnel Mach numbers below 0.6, an unusually large response on the suction surface at 0.15 chord and 0.88 radius was observed. The behavior of this response suggests the presence of a leading edge vortex. The midchord measuring stations on the suction surface exhibit a response that leads the forcing function while most other locations show a phase lag. Evidence of trailing edge shocks crossing the blade passage and impinging on the pressure surface of the following blade was found at tunnel Mach number of 0.85.

INTRODUCTION

In order to achieve the substantial fuel savings offered by an advanced turboprop over turbofan engines, cabin and community noise levels must be acceptable. The noise caused by unsteady loading of the blades can be significant source for single rotation propellers. This is the case where the axis of rotation is at angle to the inflow or where there is a distortion of the inflow caused by installation effects. The sensitivity of a single rotation propeller to inflow angle was shown to be between 0.8 to 1.6 dB per degree of inflow angle change in the flight test reported in reference 1.

In this investigation the unsteady blade surface pressures were measured on the SR-7A propeller which is a 2/9 aeroelastic scale model of the "Large-Scale Advanced Propfan" (LAP) propeller. The flight Mach number, inflow angle, and advance ratio were varied while measurements were made at nine blade stations. The limitations of scale, and the number of data channels that could be brought across the rotating interface, limited the number of measuring stations.

At a freestream Mach number of 0.8, the data are compared to an unsteady three-dimensional Euler solution. The solution procedures were developed by Whitfield, et al. (refs. 2 and 3). The solution for an inflow angle of 1.6° was reported by Nallasamy (ref. 4).

APPARATUS AND PROCEDURES

The tests were conducted in the NASA Lewis 8- by 6-Foot Supersonic Wind Tunnel over a range of Mach numbers from 0.4 to 0.85. Figure 1 shows the SR-7A propeller installed in the tunnel. The inflow angle was varied by pitching the propeller axis up. The pitch angle (inflow angle) was varied from -1° to 4°. Most of the data were obtained at an advance ratio, J, of 3.06, while limited data were obtained at J = 2.9 and J = 3.2. The blade setting angle for the tests was 60.1°. The cruise design parameters for this propeller are presented in table I.

Blade Mounted Transducers (BMT's)

Ten miniature pressure transducers were mounted on two different blades in positions shown in figure 2(a). Two chordwise stations were used at both the 0.75R and 0.88R (R = radius), while only the 0.1C (C = chord) station was used at 0.65R. The BMT's measuring the suction surface were all mounted on one blade while the pressure surface measurements were made on a second blade. The two instrumented blades were mounted in the hub 180° apart. The transducers were mounted to measure the pressure through a 1.55 mm diameter hole drilled through the blade as shown in figure 2(b). An RTV silicone adhesive was used for bonding in order to ensure that the transducers were strain isolated from the blade. The RTV adhesive was also used to fair the BMT into the blade surface.

The signals from the BMT's are taken off the rotor through a rotary transformer. Transducer excitation is a 30 kHz signal brought across the rotary transformer. The transducer output amplitude modulates the 30 kHz carrier which is demodulated, amplified, and recorded on FM tape. The system frequency response was 10 kHz or 65 to 130 shaft orders (P orders) depending on rpm.

The recorded BMT signals, along with the once-per-revolution pulse were digitized at rate of 128 samples per revolution. The digital information was then processed on a mainframe computer to produce 100 time ensembles of ten revolutions each. These were averaged synchronously to the once-per revolution pulse (time domain averaging), and fast Fourier transforms (FFT's) were taken to produce enhanced spectra and phase (azimuth) angles. In addition, FFT's were taken of the individual time ensembles of data and then averaged in the frequency domain. These spectra were only used to monitor data quality. The broadband level provided by the frequency domain average allows a check on amplifier gains, transducer health, and sets a lower limit to which the tone levels can be enhanced. All spectra produced are in terms of shaft orders (P).

RESULTS AND DISCUSSIONS

Measurements were obtained for 9 blade stations (one station on the pressure surface at 0.1C and 0.75R was not functioning). The following parameters were varied over the stated ranges: tunnel Mach number, M_∞ = 0.4 to 0.85; inflow angle, α = -1° to 4°; advance ratio, J = 2.9 to 3.2.

Typical Response to Angular Inflow

All the data presented has been averaged in the time domain synchronous to the once-per-revolution signal. The waveform (pressure versus azimuth angle) and spectrum for the suction surface at the 0.1C, 0.65R location for an inflow angle of 1.5° and M_∞ = 0.8 is shown in figure 3. All the results presented have been corrected for the residual signal at zero inflow angle. It was found that when the propeller was set at a 0° pitch angle in the tunnel there was still significant variation in the transducer signals with azimuth angle for some of the data channels. Most of this variation was at the first shaft order. It is thought that this was a result of imperfections in the windings of the rotary transformer used to transfer the signals from the rotating propeller, and some residual angular inflow. To correct for this, the first shaft order signal at zero indicated inflow angle was subtracted from the signals at all inflow angles. The reference for the azimuth angle used here is shown in figure 4 where 0° is at the top and the angle is measured in the direction of rotation (clockwise looking downstream). Thus, the maximum blade angle of attack occurs near 90° and the minimum near 270° for a positive (pitch up) inflow angle. Figure 3(a) shows that the minimum pressure occurs somewhat later than the 90° position that corresponds to the maximum blade angle of attack. The phase lag here is 26.8°. The spectrum shown in figure 3(b) is the Fourier transform of figure 3(a). The first shaft order is by far the dominant signal with the second shaft order almost an order of magnitude lower.

Comparison with Unsteady Three-dimensional Euler Solution

The unsteady three-dimensional Euler solutions at three inflow angles for the full-scale version (SR-7L) of the propeller tested here were presented in reference 4. The comparison between the Euler solution and the data will be made at individual measuring stations in terms of the unsteady pressure coefficient and azimuth angle (waveform). This is a most detailed and stringent kind of comparison. The unsteady pressure coefficient used here is the value of the unsteady pressure divided by the local dynamic pressure. Dynamic pressure was calculated from the tunnel static pressure and the vector sum of the tangential and axial velocities at the local blade radius. Some of the code conditions were slightly different than the data. The blade station locations for the code are within 2.9 percent of chord or radius of the measurement locations. The code was run at an advance ratio of 3.12 while the data was taken at J = 3.06. The inflow angle for the code was 1.6° while the data was at 1.5°. The blade setting angle for the code was 58.4° while the data was taken at 60.1°.

Comparison of the code results to the measured waveforms for the pressure surface locations are shown in figure 5. The stations at 0.1C for both the 0.65R and 0.75R (figs. 5(a) and (b)) show excellent agreement between the data

and code results. For the 0.5C and 0.88R station (fig. 5(d)) the code overpredicts the magnitude but is in good agreement with the data in phase angle. At the 0.15C and 0.88R station (fig. 5(c)) there are substantial differences between the code predictions and data. These differences involved both the shape and magnitude of the waveform. When the next higher inflow angle data (α = 2.0°) is overlaid on the figure it can be seen there is a large change in waveform shape and magnitude for the 0.5° increase in inflow angle. This and the fact that the waveform is not sinusoidal may be an indication that an unusual flow phenomenon is involved at this location and operating condition. It is interesting to note that the code results are in closer agreement with the 2° data.

The comparisons for the suction surface stations are shown in figure 6. The 0.1 chord stations at 0.65R and 0.75R (figs. 6(a) and (b)) are somewhat overpredicted in magnitude but show good agreement in phase angle. The 0.5C, 0.75R (fig. 6(c)) shows similar results to the 0.1C stations. At the 0.15C, 0.88R station (fig. 6(d)) the data for the 1.5° inflow angle was not available. Because of this the data at the next lower and higher inflow angles are shown (1.0° and 2.0°). Consistent with the code overpredicting the pressure coefficient magnitude the 2.0° data is in good agreement with the code prediction for 1.6° inflow angle. Finally, the 0.5C, 0.88R station shown in figure 6(e) shows the same overprediction in magnitude and good agreement in phase as was the case for many of the previous comparisons.

Effect of Inflow Angle

The effect of inflow angle on the unsteady pressure coefficient at the first shaft order, C_{p_1}, can be seen in figures 7 to 9. Both the magnitude and phase are shown. The magnitude of C_{p_1} is the rms value of the unsteady pressure at the first shaft order divided by the local dynamic pressure. The phase angles reported here are in terms of lead or lag from the forcing function. For a suction surface, the forcing function is considered to be negative when the blade angle of attack is positive, while the pressure surface forcing function would be positive. Figure 7 shows the inflow angle effect on C_{p_1} at a Mach number of 0.4 for all nine locations. The magnitude of C_{p_1} on the pressure surface at the stations near the leading edge have a linear response to inflow angle. The midchord stations show some nonlinear tendencies. The phase angles for all stations are similar in value (20° to 35° lag) and seem unaffected by inflow angle. On the suction surface the value of C_{p_1} for 0.15C and 0.88R has a response of more than four times (see the alternate scale on the right) the other leading edge stations and is nonlinear. This unusual behavior is a function of Mach number and will be discussed later. The midchord stations show lower but more linear response. The phase angle for both midchord stations show a lead while, the leading edge stations show a phase lag. Except for the 0.15C, 0.88R station, and 0.5C, 0.88R, the phase angle does not change with inflow angle.

Figure 8 presents the response of all stations to inflow angle at the Mach number of 0.6. The response on the pressure surface are almost the same as the M_∞ = 0.4 results for both C_{p_1} and phase angle. On the suction surface (see Fig. 8(b)), the magnitudes of C_{p_1} are similar to the M_∞ = 0.4 results, except for the 0.15C, 0.88R station which shows a large decrease. The phase of the two midchord stations show less lead, than at M_∞ = 0.4. This is particularly true for the 0.88R station.

Finally, the response at $M_\infty = 0.8$ is shown in figure 9. The pressure surface Cp_1 magnitudes of the leading edge stations are slightly reduced from the $M_\infty = 0.6$ case while the midchord stations are somewhat higher. They all exhibit a linear relation with inflow angle. The phase angles here again show little change with inflow angle except for the 2° inflow case at 0.15C, 0.88R where there is a sudden increase in lag. This is a result of a new feature in the waveform and will be discussed later. The magnitude of the Cp_1 on the suction surface is similar to that of the $M_\infty = 0.6$ data except for a lower response to inflow angle. The phase angle still shows very small change with inflow angle but the 0.5C, 0.88R station no longer leads the forcing function. It should be noted that as the Mach number was increased the maximum inflow angle that could be run was decreased due to blade stress.

Effect of Mach Number

Data were taken between $M_\infty = 0.4$ and 0.85 in 0.05 increments. The unsteady pressure coefficient at the first shaft order, Cp_1 is plotted against the blade section relative Mach number, M_r at $J = 3.06$ and inflow angle, $\alpha = 2°$ in figures 10 and 11. The magnitude and phase of Cp_1 for the pressure surface station is shown in figure 10. The magnitude of the 0.65R and 0.75R stations decreases above a relative Mach number of 0.95, while both 0.88R stations show a general trend of increasing M_r. The 0.5C, 0.88R station has a dramatic increase above $M_r = 1.1$. There is a complete change in waveform, possibly due to a shockwave from the trailing edge of blade just ahead. The waveforms for this and other unusual effects will be shown in a later section. The phase angles of the leading edge stations have a gradual decrease with increasing M_r. The midchord stations show little change in phase angle except above $M_r = 1.1$, where there is a sudden increase in lag corresponding to the waveform change.

The suction surface response to M_r is shown in figure 11. Here the most obvious feature is the high and rapidly decreasing response with increasing M_r of the 0.15C, 0.88R station. The reason for this high response is not known but may be caused by a leading edge vortex. This kind of high and rapidly changing response has been seen on this propeller before at takeoff conditions (ref. 5). It was not expected that a leading edge vortex would play any role at cruise conditions. The other two leading edge stations have very similar response to each other with Cp_1 in the 0.06 range up to $M_r = 0.95$ then decreasing at higher M_r. The phase response to M_r for the three leading edge stations is similar, with increasing lag with M_r. The midchord stations have phase leads at low Mach numbers with the lead decreasing with increasing M_r. The 0.5C, 0.88R station decreases its lead angle with increasing M_r to the point that it turns into a lag above $M_r = 0.85$.

Effect of Advance Ratio

The effect of advance ratio, J on the unsteady pressure coefficient at the first shaft order Cp_1 is shown in figures 12 and 13 for $M_\infty = 0.6$ and $M_\infty = 0.8$, respectively. Advance ratio is defined here as $J = V_\infty/nD$ where n is the rotational speed and D is the tip diameter. Both the magnitude and the phase of Cp_1 are shown at an inflow angle of 2°. Only three advance ratios were run, 2.90, 3.06, and 3.20.

The pressure surface stations at $M_\infty = 0.6$ are shown in figure 12(a). There are no significant trends at these stations although there is a tendency for the pressure coefficient magnitude to increase slightly with J. On the suction surface there is more activity as shown in figure 12(b). The 0.15C, 0.88R station there is a large decrease with increasing J. This is the same location that exhibited very high levels of C_{p_1} that decreased rapidly with increasing M_∞ as discussed in the previous section. This decrease in response with steady blade loading (increasing J) is consistent with a leading edge vortex. The other stations show no strong trends in C_{p_1} with J. With the exception of the 0.5C, 0.88R station which goes from a substantial phase lead at J = 2.9 to a near zero phase angle at J = 3.2; there are only small changes in phase angles with J.

The effect of J on the pressure surface measuring stations at $M_\infty = 0.8$ is shown in figure 13(a). There is a general trend for the magnitude of the pressure coefficient to decrease with increasing J. This is different from the $M_\infty = 0.6$ data where there was a slight increase with J. The only large change in phase angle occurs at the 0.15C, 0.88R station where there is a decrease in lag as J increases. The suction surface data are shown in figure 13(b) for $M_\infty = 0.8$. There are not any significant trends in either the magnitude or phase of the pressure coefficient with J. Unfortunately, the 0.15C, 0.88R station data is unavailable here.

Selected Waveforms of Unusual Effects

Examination of the waveforms at conditions where unusual response is noticed can lead to a better understanding of the phenomena responsible.

The unusually high response of the 0.15C, 0.88R station on the suction surface at low Mach numbers is examined further in figure 14. Here the waveforms in terms of C_p as a function of azimuth angle is shown for $M_\infty = 0.4$, 0.5, 0.6, and 0.7 at $\alpha = 2°$. At $M_\infty = 0.4$, the positive (minimum loading) part of the waveform has a sawtooth shape with a rapid drop past 340°. The zero crossings are over 180° apart. At $M_\infty = 0.5$ the levels of C_p are lower but with a similar sawtooth shape on the positive side of the axis. The peak has moved to a higher angle and the zero crossings are less than 180° apart (time spent below the axis is less). For $M_\infty = 0.6$ there is a large change in the shape. The sawtooth shape with the rapid drop is gone and the zero crossings are much closer together. When the M_∞ is raised to 0.7 there is again another major change in shape. The zero crossings here now move in the opposite direction, over 200° apart (more time spent below the axis). As has been pointed out earlier, the magnitude of C_p decreases rapidly with increasing M_∞. Nothing definitive can be said as to the source of these waveforms and the evolution with M_∞, but similarity has been noticed with waveforms taken at $M_\infty = 0.2$ at takeoff conditions, where a leading edge vortex seems to be present. These similarities involve the sawtooth shape above the zero pressure axis and the reduced time spent below the axis.

Another unusual area in the data is the change on the pressure surface at midchord and 0.88R station that occurs between $M_\infty = 0.8$ and 0.85 at $\alpha = 2°$. Figure 15 shows a comparison of the two waveforms. The $M_\infty = 0.8$ curve is basically a sinewave with a maximum value near 120°. Examination of the $M_\infty = 0.85$ waveform reveals much of it is parallel to the $M_\infty = 0.8$ curve. Only at two locations are there big differences: the first starting near 90° where

there is a rapid pressure rise and the second near 330° with and equally steep pressure drop. The rapid changes in pressure that created this waveform suggest a shock was involved. The unsteady Euler analysis presented in ref. 4 shows that the trailing edge shock crosses the blade passage and impinges on the pressure surface in the vicinity of midchord. Between the waveform shape and the Euler analysis it seem likely that oscillation of the trailing edge shock of the blade just ahead is responsible for the pressure response shown.

CONCLUDING REMARKS

The surface pressure response to inflow angle of the SR-7A propeller was measured at nine blade locations for Mach numbers in the cruise range. A comparison of the waveforms (unsteady pressure coefficient versus azimuth angle) to an unsteady Euler solution yielded very encouraging results considering the detailed nature of this comparison.

The code predicts the shape (phase) of the waveform very well while the magnitude is overpredicted in many cases. However, only at one measuring station, 0.15C, 0.88R on the pressure surface was there a substantial difference between the code and the data. This measuring station exhibited rapid changes in waveform with inflow angle and nonsinusodial waveforms. This behavior could be indicative of a flow phenomenon not accounted for in the code.

An unusually large response on the suction surface at 0.15 chord and 0.88 radius was observed. This response decreased rapidly as the Mach number was increased. This response also decreased with decreased loading (increasing J). A leading edge vortex is a possible cause of this behavior.

The midchord measuring stations on the suction surface exhibit a response that leads the forcing function while most other locations show a phase lag.

Evidence of trailing edge shocks crossing the blade passage and impinging on the pressure surface of the following blade was found at tunnel Mach number of 0.85.

REFERENCES

1. Bartel, H.W.; and Swift, G.: Near-Field Acoustic Characteristics of a Single-Rotor Propfan. AIAA Paper 89-1055, Apr. 1989.

2. Whitfield, D.L., et al.: Three-Dimensional Unsteady Euler Solutions for Propfans and Counter-Rotating Propfans in Transonic Flow. AIAA Paper 87-1197, June 1987.

3. Janus, J.M., and Whitfield, D.L.: A Simple Time Accurate Turbomachinery Algorithm with Numerical Solutions of Uneven Blade Count Configuration. AIAA Paper 89-0206, Jan. 1989.

4. Nallasamy, M., and Groeneweg, J.F.: Unsteady Euler Analysis of the Flowfield of a Propfan at an Angle of Attack. AIAA Paper 90-0339, Jan. 1990 (Also, NASA TM-102426).

5. Heidelberg, L.J.; and Woodward, R.P.: Advanced Turboprop Wing Installation Effects Measured by Unsteady Blade Pressure and Noise. AIAA Paper 87-2719, Oct. 1987 (Also, NASA TM-100200).

TABLE I. - UNSTEADY BLADE PRESSURE MEASUREMENTS FOR THE SR-7A PROPELLER AT CRUISE CONDITIONS

Diameter, cm (in.)	62.2(24.5)
Number of blades	8
Design Mach number	0.80
Design tip speed, m/sec (ft/sec)	244(800)
Design advance ratio	3.06
Design power coefficient	1.45
Design power loading, kW/m^2 (hp/ft^2)	257(32.0)
Integrated design life coefficient	0.202
Activity factor	227
Design efficiency, percent	79

ORIGINAL PAGE
BLACK AND WHITE PHOTOGRAPH

FIGURE 1. - SR-7A PROPELLER INSTALLED IN LEWIS 8- BY 6-FOOT WIND TUNNEL.

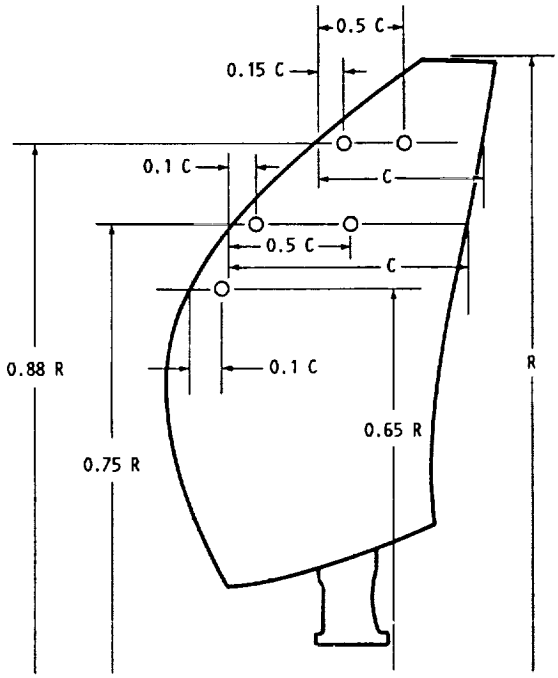

(A) PRESSURE TRANSDUCER LOCATIONS: TWO BLADES INSTRUMENTED, ONE ON PRESSURE SURFACE, THE OTHER ON SUCTION SURFACE.

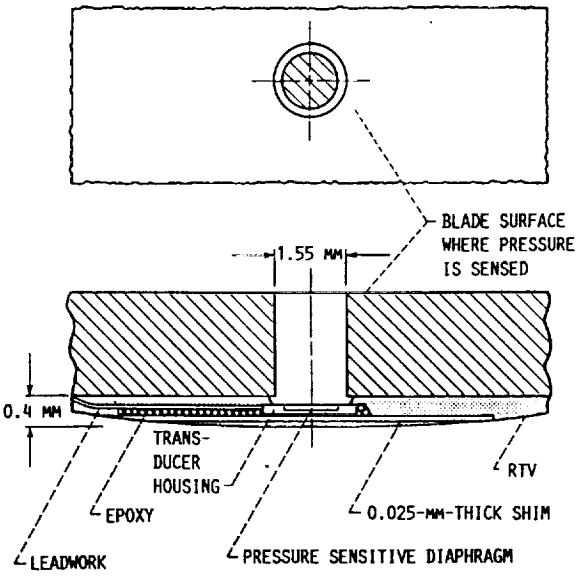

(B) TYPICAL INSTALLATION OF BLADE MOUNTED PRESSURE TRANSDUCER SENSING THROUGH BLADE.

FIGURE 2. - BLADE MOUNTED PRESSURE INSTRUMENTATION.

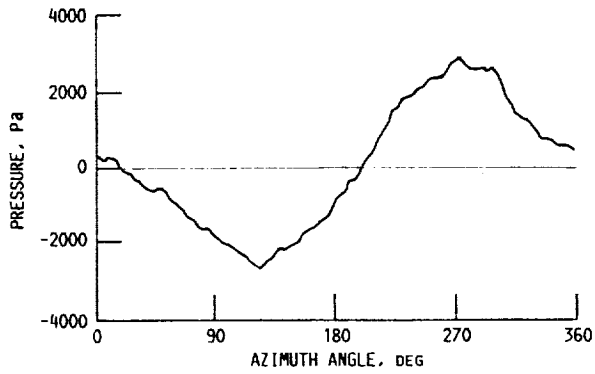

(a) TIME DOMAIN AVERAGED WAVEFORM, 100 AVERAGES.

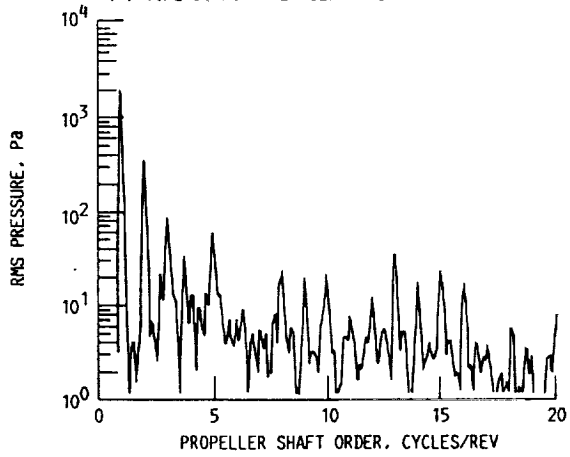

(b) SPECTRUM OF AVERAGE WAVEFORM.

FIGURE 3. - TYPICAL WAVEFORM AND SPECTRUM OF BLADE MOUNTED TRANSDUCER. LOCATION: 0.1C; 0.65R; SUCTION SURFACE. M_∞ = 0.8, α = 1.5°, J = 3.06.

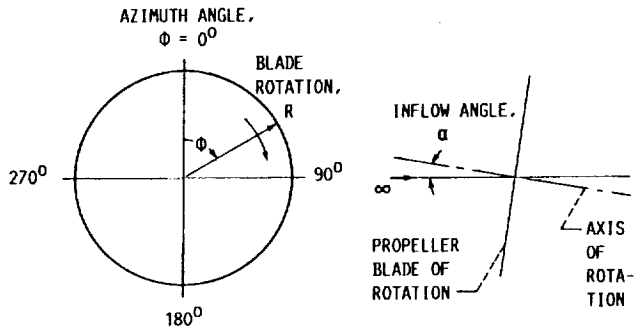

FIGURE 4. - REFERENCE GEOMETRY FOR AZIMUTH AND INFLOW ANGLES.

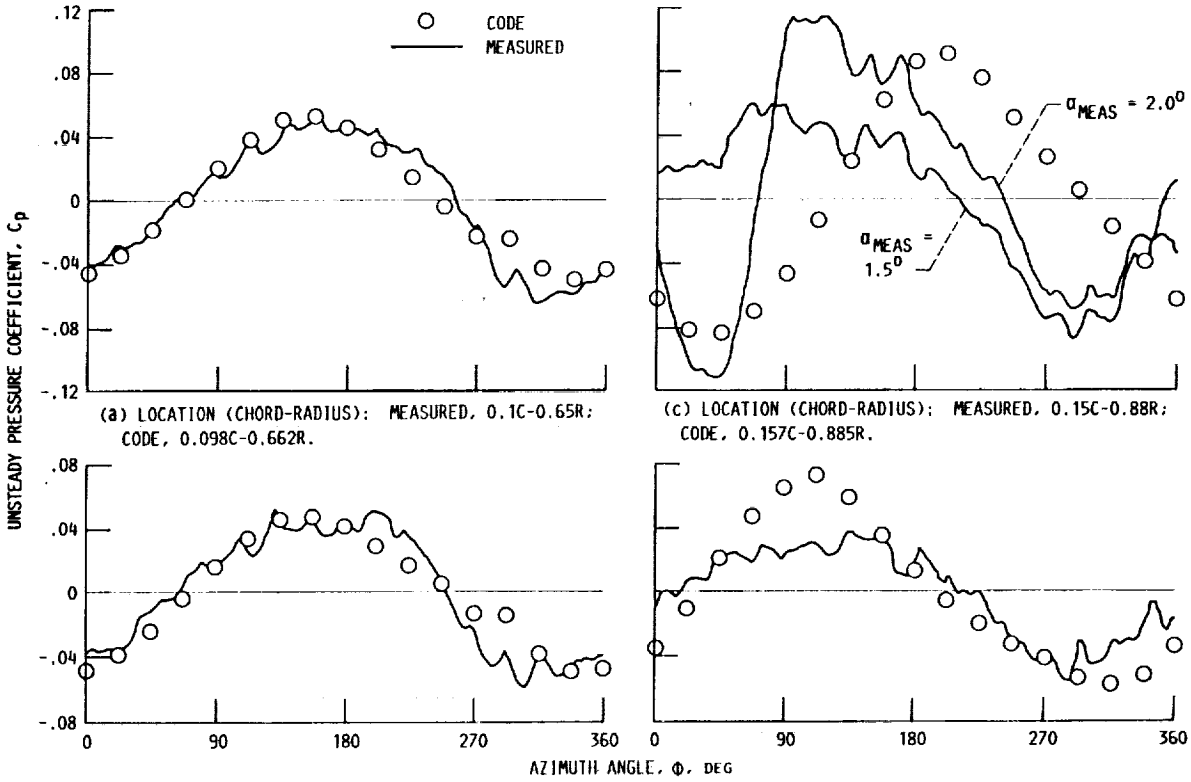

(a) LOCATION (CHORD-RADIUS): MEASURED, 0.1C-0.65R; CODE, 0.098C-0.662R.

(c) LOCATION (CHORD-RADIUS): MEASURED, 0.15C-0.88R; CODE, 0.157C-0.885R.

(b) LOCATION (CHORD-RADIUS): MEASURED, 0.1C-0.75R; CODE, 0.098C-0.736R.

(d) LOCATION (CHORD-RADIUS): MEASURED, 0.5C-0.88R; CODE, 0.529C-0.885R.

FIGURE 5. - COMPARISON OF MEASURED WAVEFORMS WITH EULER CODE SOLUTION ON THE PRESSURE SURFACE. M = 0.8; J_{MEAS} = 3.06; J_{CODE} = 3.12; α_{MEAS} = 1.5° (EXCEPT AS NOTED); α_{CODE} = 1.6°.

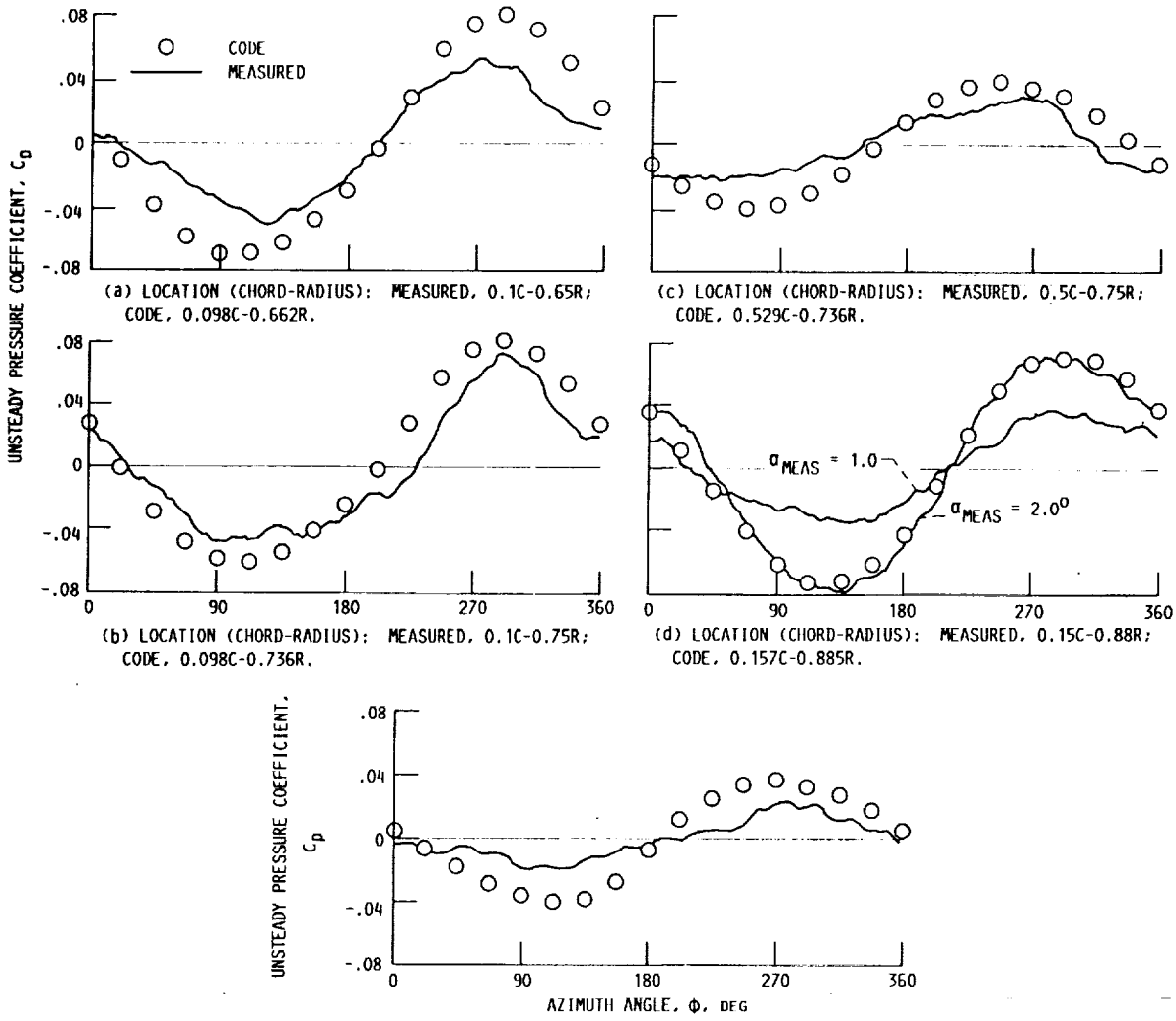

(a) LOCATION (CHORD-RADIUS): MEASURED, 0.1C-0.65R; CODE, 0.098C-0.662R.

(c) LOCATION (CHORD-RADIUS): MEASURED, 0.5C-0.75R; CODE, 0.529C-0.736R.

(b) LOCATION (CHORD-RADIUS): MEASURED, 0.1C-0.75R; CODE, 0.098C-0.736R.

(d) LOCATION (CHORD-RADIUS): MEASURED, 0.15C-0.88R; CODE, 0.157C-0.885R.

(e) LOCATION (CHORD-RADIUS): MEASURED, 0.5C-0.88R; CODE, 0.529C-0.885R.

FIGURE 6. - COMPARISON OF MEASURED WAVEFORMS WITH EULER CODE SOLUTION ON THE SUCTION SURFACE. M = 0.8; J_{MEAS} = 3.06; J_{CODE} = 3.12; α_{MEAS} = 1.5° (EXCEPT AS NOTED); α_{CODE} = 1.6°.

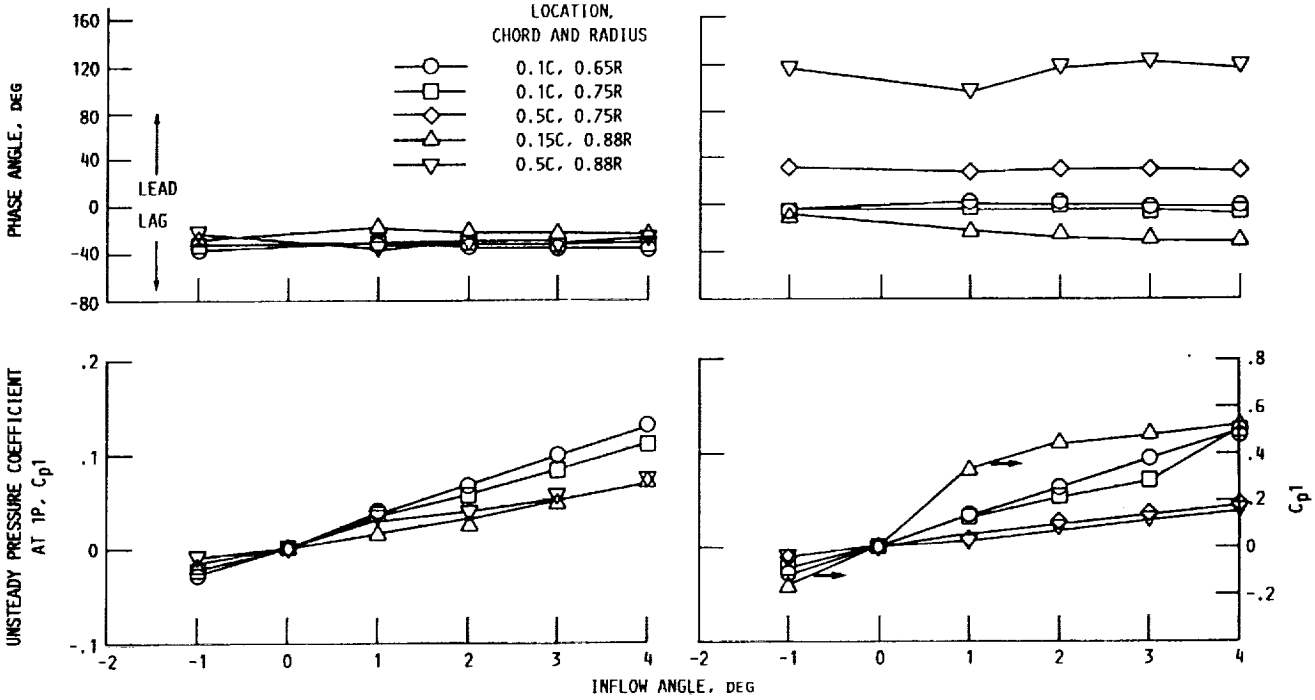

(a) PRESSURE SURFACE. (b) SUCTION SURFACE.

FIGURE 7. - PRESSURE RESPONSE AS A FUNCTION OF INFLOW ANGLE AT M_∞ = 0.4, J_{MEAS} = 3.06.

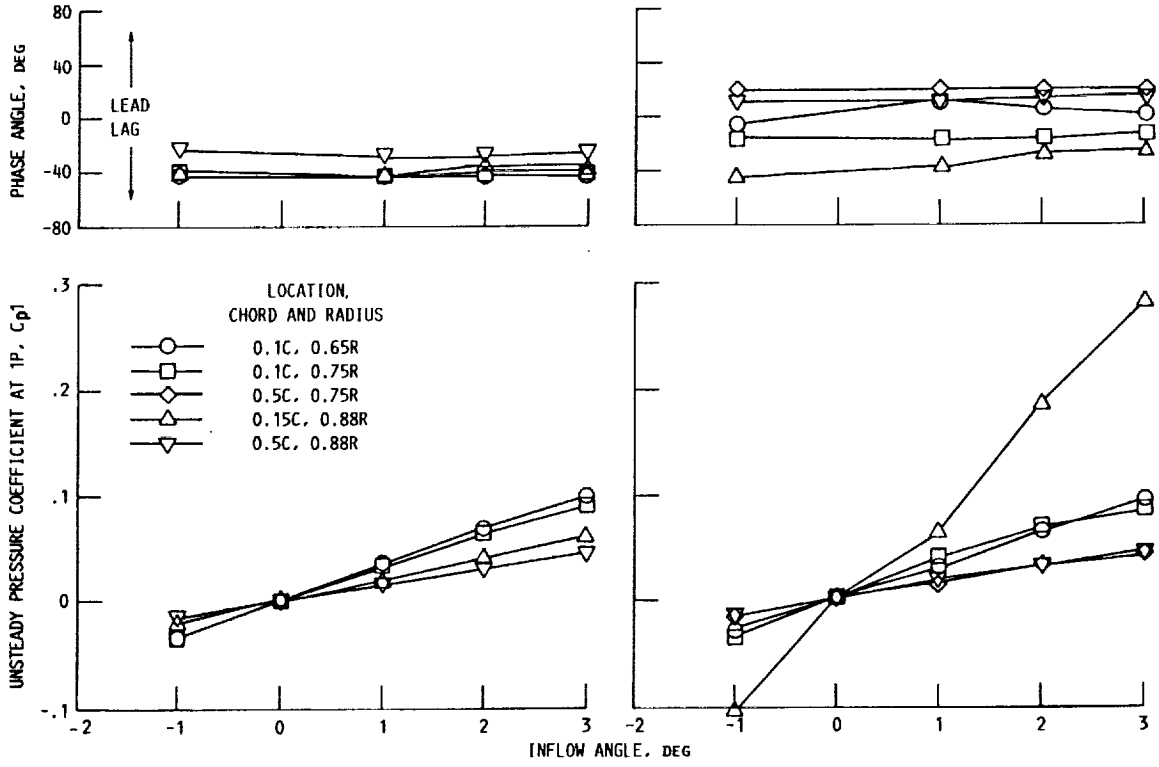

(a) PRESSURE SURFACE. (b) SUCTION SURFACE.

FIGURE 8. - PRESSURE RESPONSE AS A FUNCTION OF INFLOW ANGLE AT M_∞ = 0.6 AND J_{MEAS} = 3.06.

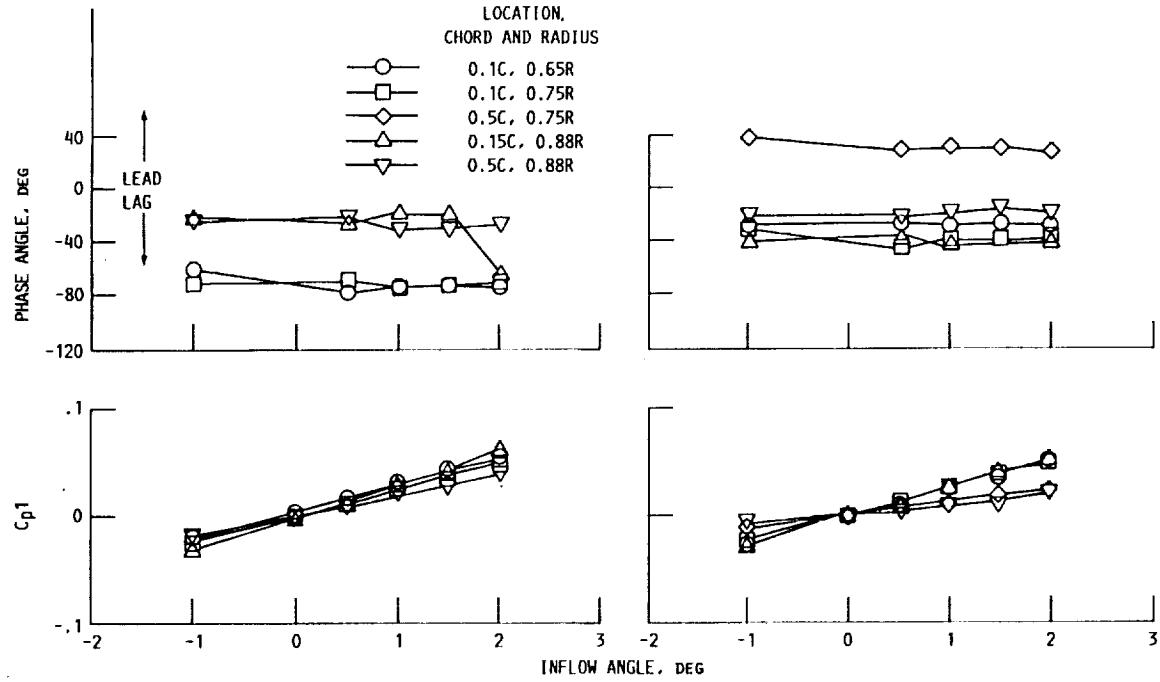

(a) PRESSURE SURFACE. (b) SUCTION SURFACE.

FIGURE 9. - PRESSURE RESPONSE AS A FUNCTION OF INFLOW ANGLE AT M_∞ = 0.8 AND J_{MEAS} = 3.06.

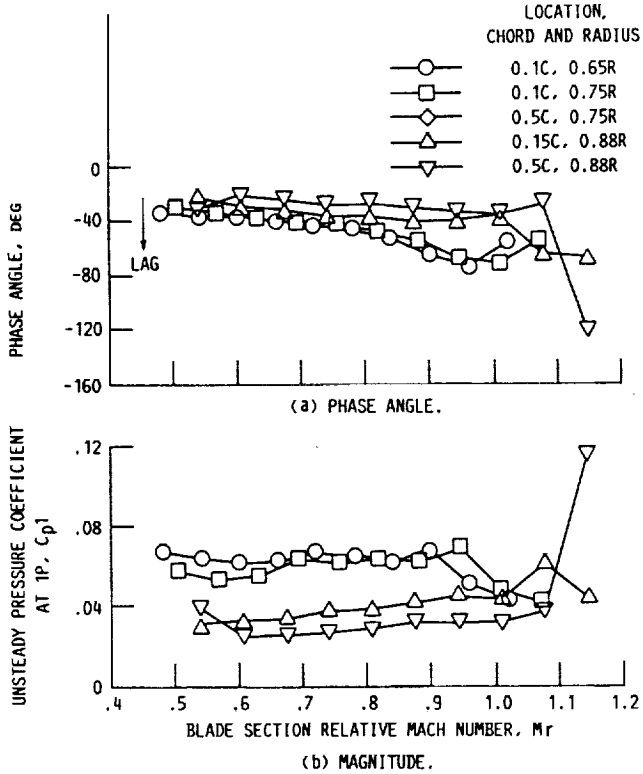

(a) PHASE ANGLE.

(b) MAGNITUDE.

FIGURE 10. - UNSTEADY PRESSURE COEFFICIENT AT THE FIRST SHAFT ORDER AS A FUNCTION OF BLADE SECTION RELATIVE MACH NUMBER. INFLOW ANGLE = 2^0; J = 3.06; PRESSURE SURFACE.

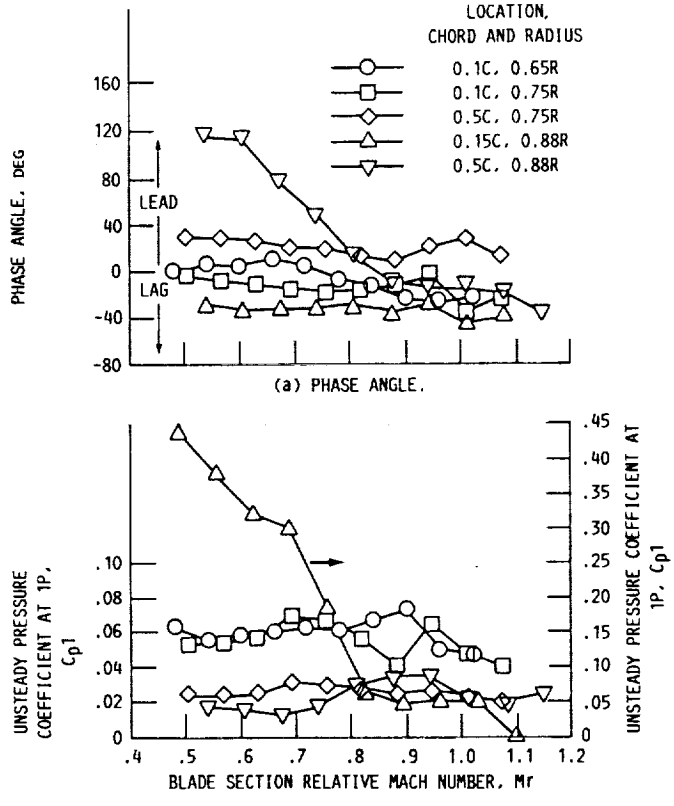

(a) PHASE ANGLE.

(b) MAGNITUDE.

FIGURE 11. - UNSTEADY PRESSURE COEFFICIENT AT THE FIRST SHAFT ORDER AS A FUNCTION OF BLADE SECTION RELATIVE MACH NUMBER, INFLOW ANGLE = 2^0, J = 3.06 SUCTION SURFACE.

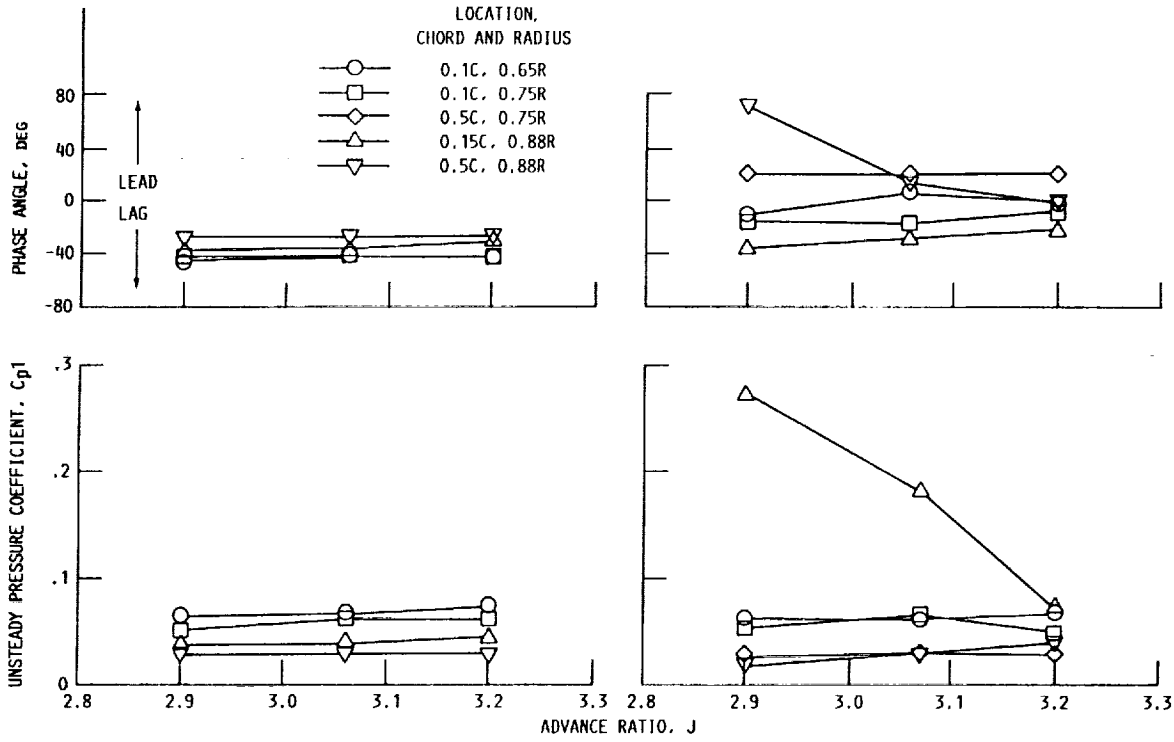

(a) PRESSURE SURFACE. (b) SUCTION SURFACE.

FIGURE 12. - UNSTEADY PRESSURE COEFFICIENT AT THE FIRST SHAFT ORDER AS A FUNCTION OF ADVANCE RATIO AT M_∞ = 0.6 AND $\alpha = 2.0^o$.

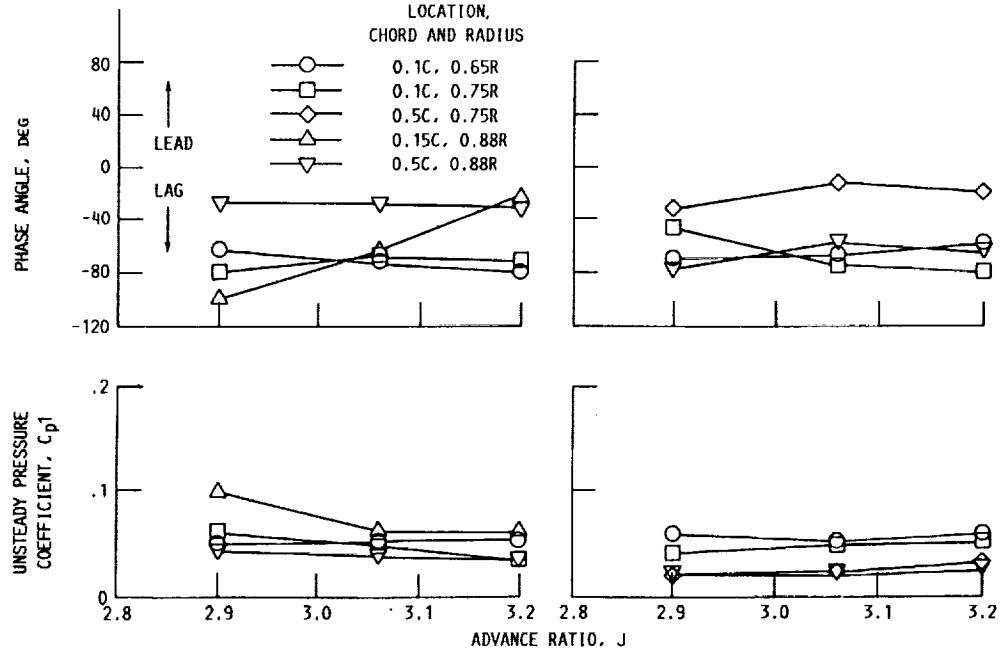

(a) PRESSURE SURFACE. (b) SUCTION SURFACE.

FIGURE 13. - UNSTEADY PRESSURE COEFFICIENT AT THE FIRST SHAFT ORDER AS A FUNCTION OF ADVANCE RATIO AT M_∞ = 0.8 AND $\alpha = 2.0^o$.

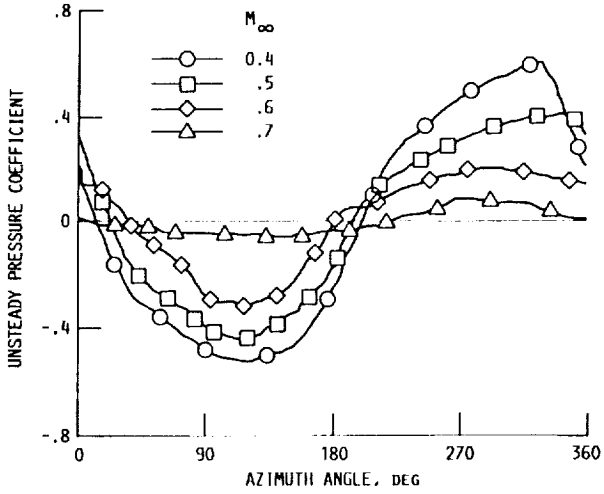

FIGURE 14. - WAVEFORMS FOR A LOCATION ON THE SUCTION SURFACE AT 0.15C AND 0.88R, $\alpha = 2^{o}$, J = 3.06.

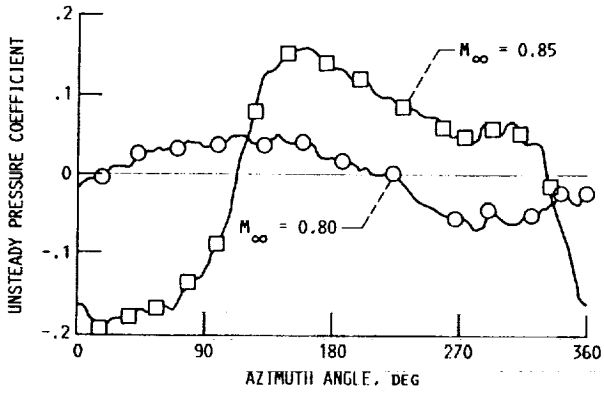

FIGURE 15. - WAVEFORMS FOR A LOCATION ON THE PRESSURE SURFACE AT 0.5C AND 0.88R, $\alpha = 2^{o}$, J = 3.06.

NASA
National Aeronautics and Space Administration

Report Documentation Page

1. Report No.	2. Government Accession No.	3. Recipient's Catalog No.
NASA TM-103606 AIAA-90-4022		

4. Title and Subtitle

Unsteady Blade Pressure Measurements
for the SR-7A Propeller at Cruise Conditions

5. Report Date

6. Performing Organization Code

7. Author(s)

L.J. Heidelberg and M. Nallasamy

8. Performing Organization Report No.

5754

10. Work Unit No.

505-62-4D

9. Performing Organization Name and Address

National Aeronautics and Space Administration
Lewis Research Center
Cleveland, Ohio 44135-3191

11. Contract or Grant No.

13. Type of Report and Period Covered

Technical Memorandum

12. Sponsoring Agency Name and Address

National Aeronautics and Space Administration
Washington, D.C. 20546-0001

14. Sponsoring Agency Code

15. Supplementary Notes

L.J. Heidelberg, Lewis Research Center. M. Nallasamy, Sverdrup Technology, Inc., Lewis Research Center Group, Brook Park, Ohio (Work done under NASA Contract NAS3-24105).

16. Abstract

The unsteady blade surface pressures were measured on the SR-7A propeller. The freestream Mach number, inflow angle, and advance ratio were varied while measurements were made at nine blade stations. At a freestream Mach number of 0.8, the data in terms of unsteady pressure coefficient vs. azimuth angle is compared to an unsteady three-dimensional Euler solution. This comparison of waveforms with the code yielded very encouraging results. The code predicts the shape (phase) of the waveform very well while the magnitude is overpredicted in many cases. At tunnel Mach numbers below 0.6, an unusually large response on the suction surface at 0.15 chord and 0.88 radius was observed. The behavior of this response suggests the presence of a leading edge vortex. The midchord measuring stations on the suction surface exhibit a response that leads the forcing function while most other locations show a phase lag. Evidence of trailing edge shocks crossing the blade passage and impinging on the pressure surface of the following blade was found at tunnel Mach number of 0.85.

17. Key Words (Suggested by Author(s))	18. Distribution Statement
Unsteady blade pressure Turboprop noise Blade-mounted transducers Installation effects	Unclassified – Unlimited Subject Category 71

19. Security Classif. (of this report)	20. Security Classif. (of this page)	21. No. of pages	22. Price*
Unclassified	Unclassified		

NASA FORM 1626 OCT 86

*For sale by the National Technical Information Service, Springfield, Virginia 22161